Research Article

Advances in Mechanical Engineering

Advances in Mechanical Engineering
2015, Vol. 7(6) 1–11

DOI: 10.1177/1687814015589533
aime.sagepub.com
SAGE

Nonlinear dynamical model of an automotive dual mass flywheel

Lei Chen, Rong Zeng and Zhengfeng Jiang

Abstract

The hysteresis, stick–slip, and rotational speed-dependent characteristics in a basic dual mass flywheel are obtained from a static and a dynamic experiments. Based on the experimental results, a nonlinear model of the transferred torque in this dual mass flywheel is developed, with the overlying form of nonlinear elastic torque and frictional torque. The nonlinearities of stiffness are investigated, deriving a nonlinear model to describe the rotational speed-dependent stiffness. In addition, Bouc–Wen model is used to model the hysteretic frictional torque. Thus, the nonlinear 2-degree-of-freedom system of this dual mass flywheel is set up. Then, the Levenberg–Marquardt method is adopted for the parameter estimation of the frictional torque. Finally, taking the nonlinear stiffness in this model into account, the parameters of Bouc–Wen model are estimated based on the dynamic test data.

Keywords

Hysteresis, dual mass flywheel, rotational speed dependent, nonlinear modeling, parameter estimation

Date received: 2 December 2014; accepted: 13 March 2015

Academic Editor: Ioan Pop

Introduction

The reciprocating internal combustion engines are used in almost every automotive vehicle recently. The oscillated gas-pressure torque caused by the periodic combustion processes and the unbalanced inertia torque excites the driveline, which generates the torsional vibrations. Torsional vibrations in automotive vehicle bring a number of comfort problems, namely, "rattle noise." Torsional vibrations transmitted from engines can be mechanically isolated when a dual mass flywheel (DMF) is fitted between the engine and transmission.[1]

A basic DMF consists of two separated flywheels connected by a spring-damping damper, as shown in Figure 1. The long-travel arc springs are compressed or decompressed along the shell, transferring the torque from engine. To reduce wear, lubricating grease is filled in spring channel, generating damping as well. A applicable model of DMF is significant to predict the dynamic behaviors of power train. Walter et al.[2–4] and Lei et al.[5] have simplified a DMF as a 2-degree-of-freedom system, which is a linear mass–spring–damper model. Using this model, the torsional vibration characteristics of the power train fitted with the DMF are predicted. However, Schnurr[6] has observed nonlinear dynamical phenomenon as early as 1990. A dynamic test for a super-long-travel DMF was conducted, and frictional hysteresis as well as the rotational speed-dependent characteristic was found. Before long-travel DMF, Albers[7] established a static mechanic model for a long-arc spring with a DMF, considering the friction in 1994, and investigated the hysteresis phenomenon under static condition. In 2009, Schaper et al.[8] also represented the nonlinear characteristics of an arc spring

School of Mechanical and Electronic Engineering, Wuhan University of Technology, Wuhan, China

Corresponding author:
Rong Zeng, School of Mechanical and Electronic Engineering, Wuhan University of Technology, Wuhan 430070, China.
Email: zengrong@whut.edu.cn

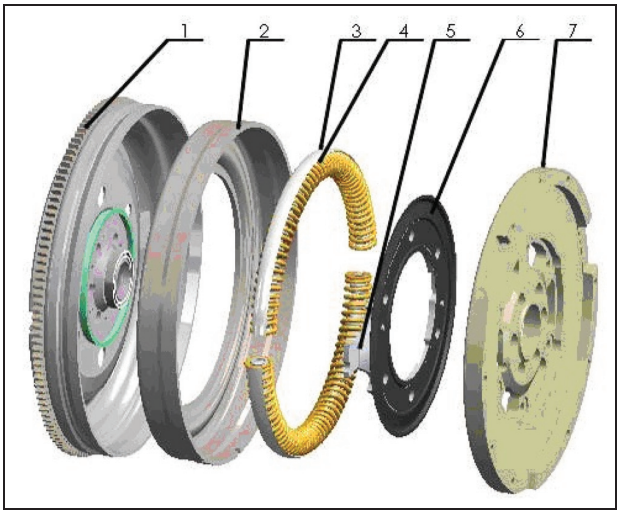

Figure 1. Schematic diagram of basic dual mass flywheel (DMF).
1: primary flywheel; 2: cover; 3: shell; 4: long-travel arc springs; 5: flange; 6: seal disk; 7: secondary flywheel.

DMF and observed the friction behavior. Although the nonlinear characteristic has been observed, the practicable model for basic DMF has not been achieved yet.

Since the DMF cannot be primitively explained by the linear dynamical model, a nonlinear model that can predict the nonlinear characteristics of DMF needs to be developed. Therefore, this work develops a nonlinear model for a typical arc spring DMF, based on the static and dynamic experiments.

Nonlinear phenomenon

In this section, a static and a dynamic experiments of an arc spring DMF are represented. The torque from engine may take the form as

$$T_{\text{eng}} = T_0 + \sum_{j=1}^{\infty} \Delta T_j \cdot \cos\left(j\omega_0 t + \psi_j\right) \qquad (1)$$

where T_{eng} is the torque from engine; T_0 is the mean torque that is practically needed; ΔT_j and ψ_j are the oscillation amplitude and the phase angle of the number j order, respectively; and ω_0 is the base frequency, representing the rotational speed. Due to the engine torque, the arc spring will be compressed with oscillation. Since $T_0 \gg \Delta T_i$, the stiffness is mainly influenced in the stable loading process without oscillation. However, the damping characteristic should be studied at dynamic status.

Figure 2 shows the experimental setup for the DMF. The DMF is excited by a converter motor, which is controlled by a specified transducer. The harmonic excitation frequency is equal to the base frequency, that

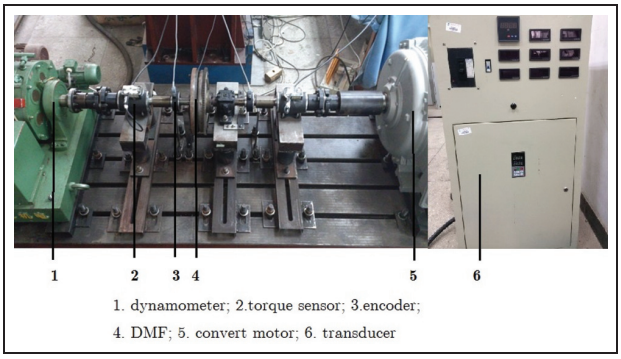

Figure 2. Experimental setup.
1: dynamometer; 2: torque sensor; 3: encoder; 4: DMF; 5: converter motor; 6: transducer.

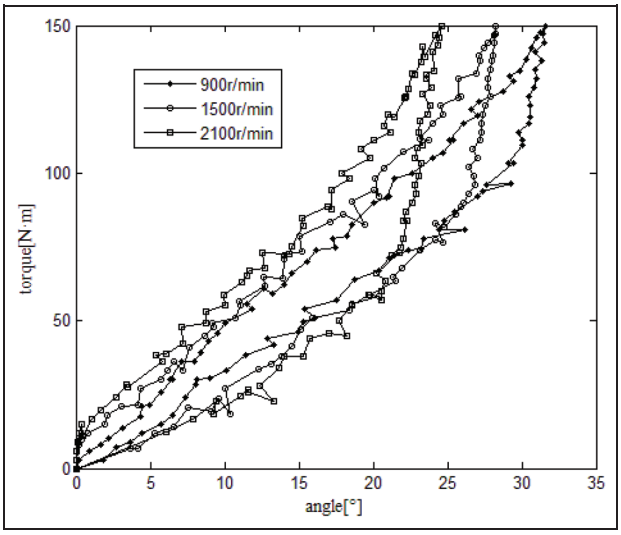

Figure 3. Torque–angle curves from static experiment.

is, $j = 1$. The load imposed on the DMF is achieved by a dynamometer. The torque transferred by the DMF and torsional displacements of the primary and the secondary flywheels are detected by torque sensors and encoders, respectively. With respect to the static experiment, the excitation is unused, and the load is controlled to increase linearly from 0 to 150 N m and then reduce to 0 N m. The relation between the torque transferred and the torsional angle differences is plotted in Figure 3, under several stable rotational speeds. For dynamic experiment, the excitation amplitude is set to be 10 N m, and the excitation frequencies corresponding to the rotational speed are 15, 25, and 35 Hz, respectively. In this case, the loads imposed on the DMF are controlled to be 80 and 120 N m. The dynamic torque–torsional angle curves are plotted in Figure 4.

Hysteresis phenomenon is observed in both static and dynamic experiments. The area enclosed by a

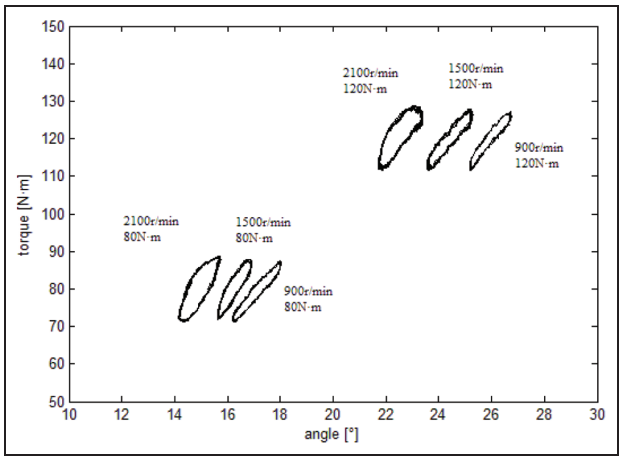

Figure 4. Torque–angle curves from dynamic experiment.

complete loop denotes the energy dissipated. The curves in Figures 3 and 4 show that the areas enclosed change as the rotational speed changes, increasing with the increase in the rotational speed. Figure 3 also shows that the stick–slip phenomenon occurs. The arc springs stick again to the shell until the external torque is large enough to overcome the static friction. What is more, the stiffness increases with the increase in the rotational speed in loading processes. Furthermore, in Figure 4, the leans of the curves become steeper as the rotational speed increases, indicating that the stiffness enlarges with the increase in rotational speed. Thus, it is observed that the torque transferred by the DMF is rotational speed dependent.

Modeling the DMF

The DMF can be modeled as a 2-degree-of-freedom system, but the stiffness and the damping are no longer linear, according to the observation. The moments of inertia of the primary and secondary flywheels can be demonstrably solved as constant. While the transferred torque from the arc springs needs to be accurately analyzed, due to the observed nonlinear phenomenon. Thus, we can consider that the transferred torque consists of two nonlinear parts from spring torque and the friction, which may be described as

$$T(t) = K \cdot \theta(t) + z(t) \tag{2}$$

where $T(t)$ is the total restoring torque or the transferred torque, K is the nonlinear stiffness, and $z(t)$ is the nonlinear frictional torque. First, the nonlinearity of the stiffness will be investigated.

Nonlinearity of the stiffness

In this section, the forces acting on the arc spring are observed. The discrete method is used, which means

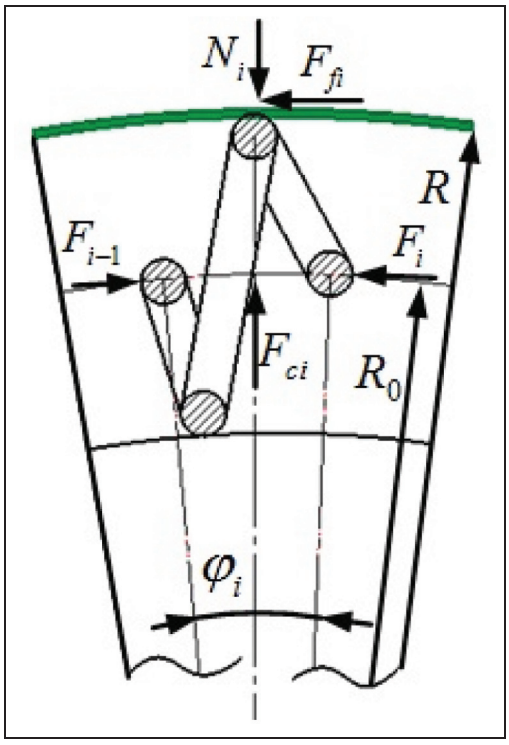

Figure 5. Free-body diagram of coil *i*.

that the whole arc spring is dispersed to spring coils. When using this method, three assumptions listed below should be followed:

1. Each spring coil is linear, referring to the linear spring design method;
2. Directions of each coil deformation are consistent, which are circumferential;
3. The friction force between the spring and spring holder is uniform.

The whole arc spring was dispersed to n coils. In addition, the spring coils produce deformation being subjected to elastic forces caused by the previous spring coil and the next one, when external force is imposed on the arc spring. The elastic forces result in radial redirection force, which combines with the radial centrifugal force to generate the radial normal force. The normal force leads to the spring coil contacting with the shell, thus producing the coulomb friction force. Figure 4 shows the free-body diagrams of the number i coil.

In Figure 5, F_{i-1} and F_i denote the elastic forces caused by the number $i-1$ coil and $i+1$ coil, respectively, where $i = 1, 2, \ldots, n$. F_0 represents the external force. N_i, F_{fi}, and F_{ci} are normal force, frictional force, and centrifugal force, respectively. φ_i describes the circumferential distribution angle of this coil under the compressed condition. R_0 and R denote the

intermediate distribution radius and the outer distribution radius of the whole arc spring, respectively. Note that units of above forces, angles, and radii are given by Newton, radian, and meter, respectively.

The shells in the circumferential spring dual mass flywheel (DMF-CS) guide the circumferential movement of the arc springs and then the friction will act on the contacting surfaces. Lubricating grease is filled in spring channel, reducing wear of the arc springs and generating damping. The lubricating stage determines the status of friction of two contacting surfaces.[9] Only the relative velocity of the contacting surfaces is high enough can they separate totally and hydrodynamic lubrication form, according to the Stribeck lubricating curve.[10] As is non-Newton fluid, the rheology of the lubricating grease characterizes nonlinearity. Under dynamic condition, the relative velocity is the torsional vibration speed. Because the friction damping consumes the energy, the vibration amplitude will be weakened. Therefore, the springs and slide may be difficult to be completely separated, and the hydrodynamic oil film cannot be fully formed. Under static condition, the relative velocity is lower. Therefore, the friction can be taken as dry friction.

Since the direction of the dry friction force is always opposite to the direction of the spring coil movement, the static mechanic model of the spring coil can be derived as follows

$$\begin{cases} (F_{i-1} - F_i)\cos\left(\frac{\varphi_i}{2}\right) = F_{fi} \\ N_i = (F_{i-1} + F_i)\sin\left(\frac{\varphi_i}{2}\right) + F_{ci} \\ F_{fi} = fN_i\, sign(F_{i-1} - F_i) \\ F_{ci} = m_i R_0 \omega^2 = \frac{\rho\pi^2 D d^2 R_0 \omega^2}{4} \end{cases} \tag{3}$$

where m_i is the mass of the number i coil and ρ is the density of the arc spring. Besides, ω (rad/s) is the rotational speed of the flywheel and f is the dry friction coefficient.

According to the first assumption, the elasticity of the spring coil is linear. Assume that the linear stiffness of the spring coil is k, the circumferential distribution angle under compressed can be expressed as

$$\varphi_i = \varphi_0 - \frac{F_{i-1}}{k \cdot R_0} \tag{4}$$

According to the linear spring theory,[11] k can be obtained from the following equation

$$k = \frac{GD^3}{8d^4} \tag{5}$$

where G is the shear modulus of the spring material, D is the intermediate diameter of the spring, and d is the diameter of the spring wire.

Assume that ϕ is the circumferential distribution angle of the whole arc spring under uncompressed condition, hence, $\varphi_0 = \phi/n$. Consider θ is the total torsional angle of the whole arc spring, which can be written as

$$\theta = \sum_{i=1}^{n} (n\phi_0 - \phi_i) \tag{6}$$

From equations (4) and (6), θ may be expressed as

$$\theta = \frac{\sum_{i=1}^{n} F_{i-1}}{k \cdot R_0} \tag{7}$$

The recurrence formula of elastic forces of the spring coils can be derived from equation (3). However, when the external torque is too small to overcome the friction force, the spring coil stays stick. Hence, the static friction should be taken into account. In this case, the static mechanic model of the spring coil is shown as

$$\begin{cases} F_{i-1}\cos\left(\frac{\phi_i}{2}\right) = F_{s1} \\ F_i = 0 \end{cases} \tag{8}$$

where F_{s1} is the static friction force. The static friction force increases with the increase in external force until it is equal to the kinetic friction force. After this, the stick spring coils become slip. In this case, $F_{i-1}\cos(\varphi_i/2) \geq F_{fi}$ and $F_{i-1} > F_i$. In accordance with equation (4), F_i can be given by

$$F_i = \frac{\left(\cos\left(\frac{\varphi_i}{2}\right) - f\sin\left(\frac{\varphi_i}{2}\right)\right) \cdot F_{i-1} - fF_{ci}}{\cos\left(\frac{\varphi_i}{2}\right) + f\sin\left(\frac{\varphi_i}{2}\right)} \tag{9}$$

Combining equation (8) with equation (9), under the loading condition, the elastic forces transferred between spring coils can be derived as

$$F_i = \begin{cases} \frac{\left(\cos\left(\frac{\varphi_i}{2}\right) - f\sin\left(\frac{\varphi_i}{2}\right)\right) \cdot F_{i-1} - fF_{ci}}{\cos\left(\frac{\varphi_i}{2}\right) + f\sin\left(\frac{\varphi_i}{2}\right)}, & \text{when } F_{i-1}\cos\left(\frac{\varphi_i}{2}\right) \geq F_{fi} \\ 0, & \text{when } F_{i-1}\cos\left(\frac{\varphi_i}{2}\right) < F_{fi} \end{cases} \tag{10}$$

In decompression process, the initial status of the arc spring is just the final status of the arc spring under the loading process. Thus, both F_i and F_{i-1} are described in equation (10). When F_{i-1} is decreasing but F_{i-1} is still greater than F_i, the spring coil is subjected to the static friction force with the same direction as F_i, then

$$(F_{i-1} - F_i)\cos\left(\frac{\varphi_i}{2}\right) = F_{s2} \tag{11}$$

where F_{s2} is the static friction force under decompression process. F_{i-1} continues to decrease until F_{i-1} is smaller than F_i. On this occasion, the arc spring begins to be decompressed. The static friction force transforms into the kinetic friction with the same direction as F_{i-1}. Thus, the recurrence formula can be written as

Table 1. Parameters of the arc spring.

Parameter	Value
Density of ρ (kg/m^3)	7850
Young's modulus E (Pa)	2E11
Shear modulus G (Pa)	7.85E10
Spring diameter D (mm)	21.5
Wire diameter d (mm)	5.2
Spring radius R_0 (mm)	127.5
Circumferential distribution angle ϕ (°)	153
Number of coils n	54

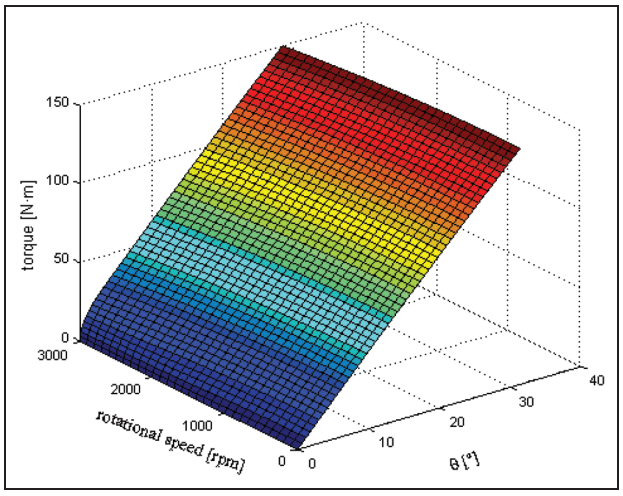

Figure 6. Relation of torque, torsional angle, and rotational speed under loading process.

$$F_i = \frac{\left(\cos\left(\frac{\varphi_i}{2}\right) + f\ \sin\left(\frac{\varphi_i}{2}\right)\right) \cdot F_{i-1} + fF_{ci}}{\cos\left(\frac{\varphi_i}{2}\right) - f\ \sin\left(\frac{\varphi_i}{2}\right)} \tag{12}$$

Therefore, under the decompression process, the elastic forces transferring between the spring coils can be summarized as

$$F_i = \begin{cases} \frac{\left(\cos\left(\frac{\varphi_i}{2}\right) + f\ \sin\left(\frac{\varphi_i}{2}\right)\right) \cdot F_{i-1} + fF_{ci}}{\cos\left(\frac{\varphi_i}{2}\right) - f\ \sin\left(\frac{\varphi_i}{2}\right)}, & \text{when } F_i \geq F_{i-1} \\ \frac{\left(\cos\left(\frac{\varphi_i}{2}\right) - f\ \sin\left(\frac{\varphi_i}{2}\right)\right) \cdot F_{i-1,\,\max} + fF_{ci}}{\cos\left(\frac{\varphi_i}{2}\right) + f\ \sin\left(\frac{\varphi_i}{2}\right)}, & \text{when } F_i < F_{i-1} \end{cases} \tag{13}$$

where $F_{i-1,\,\max}$ is the final value of F_{i-1} under the loading process.

The parameters of the arc spring of this DMF are given in Table 1. Based on the above derivation, the relation of torque, angle, and rotational speed is simulated in Figure 6. The result shows that the transferring torque is approximately linear to the torsional angle but is nonlinear to the rotational speed. Obviously, the rotational speed-dependent torque results from the friction. The friction is taken as coulomb friction in the simulation, which is induced by the normal force. Moreover, the centrifugal force and the redirection force compose the normal force. The transferring torque can be expressed as the form of the combination of the friction torque with the linear elastic torque. For practical condition, the friction torque is regarded as the mixed friction torque consisted of viscous friction torque and coulomb friction torque. Hence, the model of transferred torque in this case can be described as

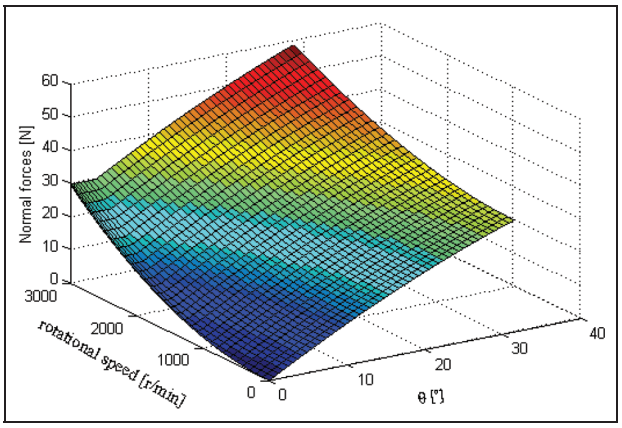

Figure 7. Variation of the normal forces.

$$T(\theta, \dot{\theta}, \omega) = \kappa \cdot \theta + c \cdot \dot{\theta} + T_N(\theta, \dot{\theta}, \omega) \tag{14}$$

where c is the viscous damping constant, κ is the linear spring constant, and $T_N(\theta, \dot{\theta}, \omega)$ is the frictional torque from normal force.

The variations of the normal force and the redirection force with the torsional angle θ and the rotational speed changing are shown in Figures 7 and 8, respectively. The results show that the normal force is approximately linear with the torsional angle but nonlinearly increases with the increase in the rotational speed. Meanwhile, the redirection force is approximately proportion to the torsional angle but decreases with the decrease in the rotational speed. Therefore, the friction torque from the normal force will satisfy the following relations

$$\begin{cases} \frac{\partial T_N}{\partial \omega_2} > \frac{\partial T_N}{\partial \omega_1} > 0, & \text{when } \omega_2 > \omega_1 \\ \frac{\partial T_N}{\partial \theta} > 0, & \text{arbitrary } \theta \end{cases} \tag{15}$$

Thus, the coulomb frictional torque T_N can be expressed as

$$T_N(\theta, \dot{\theta}, \omega) = f(\omega) \cdot \theta \cdot sign(\dot{\theta}) \tag{16}$$

In equation (16), $f(\omega)$ is a functional problem of multi-functions, of which the form can be determined by hysteretic characteristics of this system. The following method is adopted to determine the function of

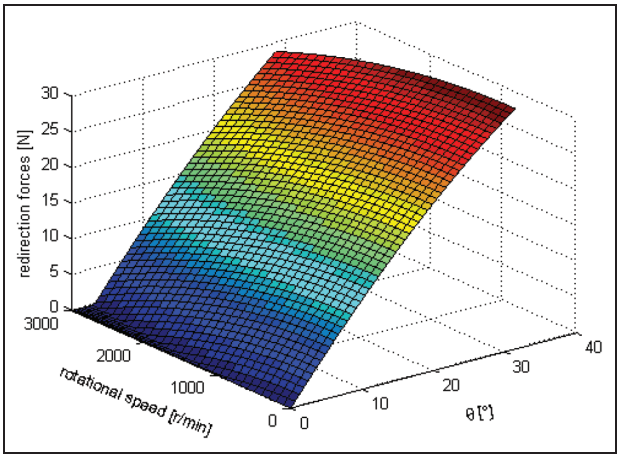

Figure 8. Variation of the redirection forces.

$f(\omega)$. First, the values of $f(\omega)$ are identified by the static experimental data from different rotational speeds. Second, the values of $f(\omega)$ are nonlinearly fitted about ω. Finally, the fitting function with the minimum error is taken as the final form of the function of $f(\omega)$.

Consequently, the final mathematical model of the transferred torque at static condition can be rewritten as

$$T(\theta, \dot{\theta}, \omega) = \kappa \cdot \theta + c \cdot \dot{\theta} + f(\omega) \cdot \theta \cdot sign(\dot{\theta}) \tag{17}$$

The transferred torque series $\{\mathbf{T}\} = \{T_1, T_2, \ldots, T_i, \ldots, T_N\}^T$ and torsional angle series $\{\theta\} = \{\theta_1, \theta_2, \ldots, \theta_i, \ldots, \theta_N\}^T$ from the static experimental data shown in section "Nonlinear phenomenon" will be used to determine the parameters of equation (17), which are κ, c, and $f(\omega)$, where $i = 1, \ldots, N$ and N is the length of the data. Besides, these two series are the same time interval, that is, Δt. The difference of the torsional angle series will substitute $\dot{\theta}$. In addition, the fourth-order accuracy difference method[12] is used to obtain the difference, as shown in equation (18)

$$\Delta\theta_i = \frac{-\theta_{i+2} + 8\theta_{i+1} - 8\theta_{i-1} + \theta_{i-2}}{12\Delta t} \tag{18}$$

Assume $\eta = f(\omega)$, thus the parameters to be determined are $\{\mathbf{y}\} = \{\kappa, c, \eta\}^T$, and the independent variable is $\{\mathbf{x}\} = \{x_1, x_2, x_3\}^T$, where $x_1 = \theta$, $x_2 = \dot{\theta}$, and $x_3 = \theta \cdot sign(\dot{\theta})$. The least square method is applied to estimate the parameters. Hence, the problem is transferred to

$$\min E(\mathbf{y}) = \sum_{k=1}^{m} \left(\mathbf{x_j^T y} - \mathbf{T}_j\right)^2 \tag{19}$$

where $\mathrm{x_j} = \{x_{1j}, x_{2j}, x_{3j}\}$ and m is the number of equations. Using the least square method, the parameters will be estimated by the following equation

$$\hat{\mathbf{y}} = \left(\mathbf{A^T A}\right)^{-1} \mathbf{A}^T \mathbf{b} \tag{20}$$

where

$$\mathbf{A} = \begin{bmatrix} \mathbf{x}_1^T \\ \mathbf{x}_2^T \\ \vdots \\ \mathbf{x}_m^T \end{bmatrix}$$

and

$$\mathbf{b} = \begin{bmatrix} T_1 \\ T_2 \\ \vdots \\ T_m \end{bmatrix}$$

Choosing appropriate values of m at each rotational speed, the estimated parameters are listed in Table 2.

Consider the mean value of parameters k and c. It is computed that $\kappa = 235.65\,\mathrm{N\,m/rad}$ and $c = 0.0127\,\mathrm{N\,m\,s/rad}$. Moreover, the values of η at each rotational speed are plotted in Figure 9.

Three nonlinear functions of ω shown in equation (21) are used to fit the data points of η. The fitting curves are illustrated in Figure 10. Parameters of a and b in each function and fitting errors are predicted based on the fitting results, as listed in Table 3

$$\begin{cases} \eta = a\left(\sinh\left(\frac{\omega}{b}\right) + 1\right) & \text{(19a)} \\ \eta = a \cdot e^{\frac{\omega}{b}} & \text{(19b)} \\ \eta = a \cdot \left(\left(\frac{\omega}{b}\right)^2 + 1\right) & \text{(19c)} \end{cases} \tag{21}$$

In Table 3, SSE, R^2, and RMS represent the sum of squares due to error, the coefficient of determination, and the root mean squared error, respectively. The fitting results show that the third function describes the variation of η the most precisely. Thus, the transferred torque model can be obtained as

$$T(\theta, \dot{\theta}, \omega) = 235.65\theta + 0.0127\dot{\theta} + 11.15\left(\left(\frac{\omega}{104.9}\right)^2 + 1\right)\theta\, sign(\dot{\theta}) \tag{22}$$

From equation (22), the transferred torque under 900, 1500, and 2100 r/min is plotted in Figure 11, which are compared with the static experimental results shown in section "Nonlinear phenomenon" as well. The results show that the established torque is available to describe the nonlinear transferred torque of the DMF.

Since the amount of viscous damping coefficient is relatively small, the torque from the viscous damping is neglected. Therefore, the nonlinear stiffness of the DMF subjected to a static torque is shown as (Figure 12)

Table 2. Estimated parameters at different rotational speeds.

Rotational speed (r/min)	m	κ (N m/rad)	c (N m s/rad)	η (N m/rad)
450	34	233.0791	0.0107	9.5021
600	28	235.0865	0.0121	12.0745
750	21	242.5641	0.0115	14.6126
900	23	231.0634	0.0145	20.9360
1050	24	236.9087	0.0127	22.3761
1200	26	237.1217	0.0134	26.8971
1350	23	241.2314	0.0121	33.1456
1500	31	230.1653	0.0119	38.7913
1650	25	228.7645	0.0129	43.9023
1800	31	236.1809	0.0131	47.4567
1950	34	239.1562	0.0121	54.7924
2100	27	229.0687	0.0142	62.9813
2250	26	231.1254	0.0136	69.8016
2400	37	230.7653	0.0127	76.2562
2550	36	245.2534	0.0119	84.8625
2700	41	234.1278	0.0134	93.1587
2850	46	248.9873	0.0125	100.8734
3000	43	231.0965	0.0138	107.7843

Table 3. Parameters of each function and the errors of curve fitting.

Function	a	b	SSE	R^2	RMS
(19a)	12.63	112.2	408.9871	0.9756	5.0558
(19b)	11.68	137.6	261.1720	0.9844	4.0402
(19c)	11.15	104.9	98.5975	0.9941	0.4824

SSE: sum of squares; RMS: root mean square.

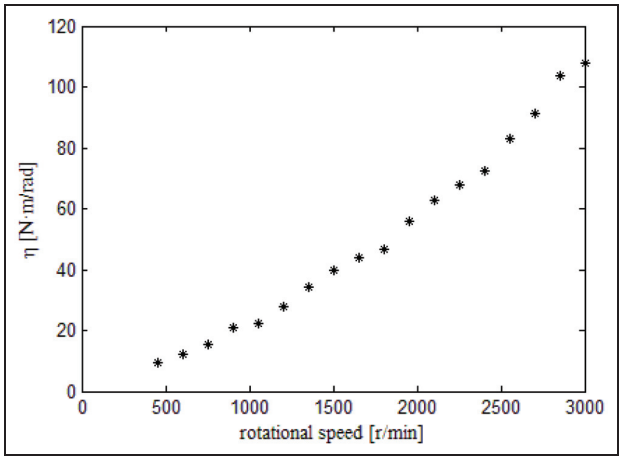

Figure 9. Values of η.

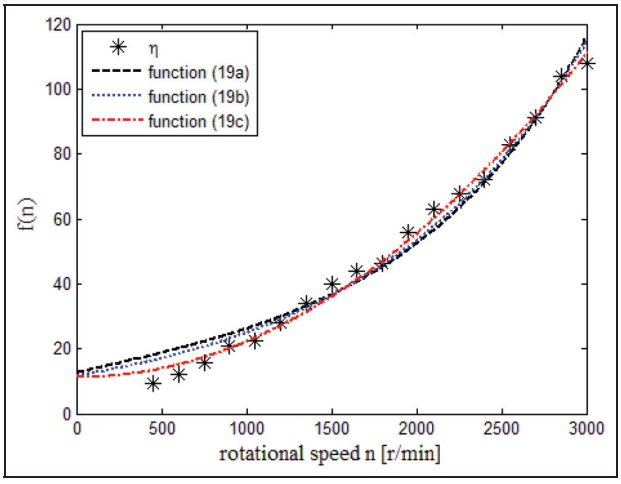

Figure 10. Curve fitting results of η.

$$K(\omega) = 235.65 + 11.25\left(\left(\frac{\omega}{104.9}\right)^2 + 1\right) \quad (23)$$

Nonlinearity of the frictional torque

The most widely used nonlinear hysteresis model is Bouc–Wen model. Bouc[13] first proposed the differential model to describe nonlinear hysteresis in 1967. Then, Wen[14] modified the model in 1976, which is Bouc–Wen model. The model can be used to predict various types of hysteretic behaviors. Adjusting the parameters of this model, we can obtain different shapes of the hysteresis. Here, the Bouc–Wen model has been employed to

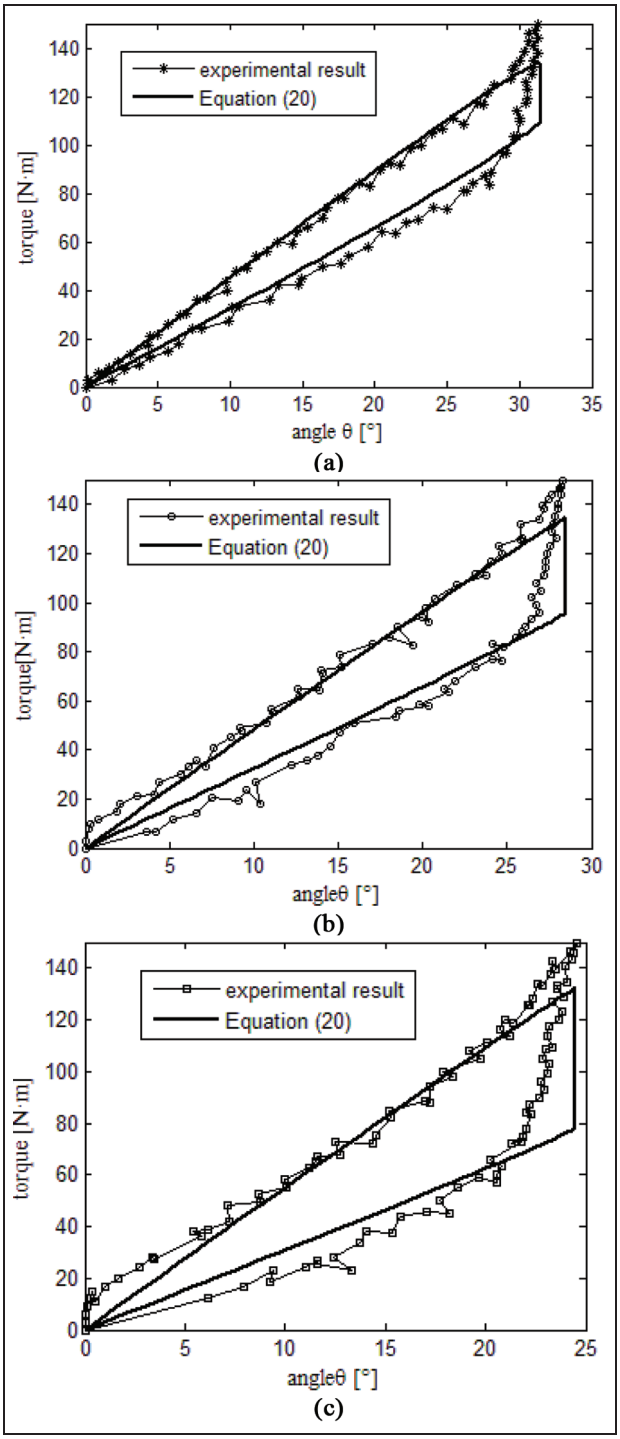

Figure 11. Comparisons of torques from experimental results and equation (22): (a) 900, (b) 1500, and (c) 2100 r/min.

model the frictional torque. Therefore, the nonlinear 2-degree-of-freedom model can be described in Figure 13, where T_{eng} is the torque from engine, in the dynamic test, which is substituted by the torque detected by the torque sensor at the front end of the primary flywheel; θ_1 and θ_2 are the torsional angles of the primary and secondary flywheels, respectively; and J_1 and J_2 are the

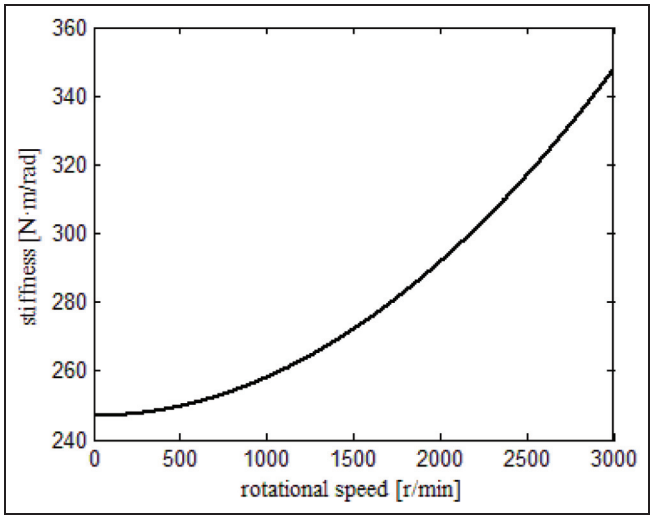

Figure 12. Variation of stiffness.

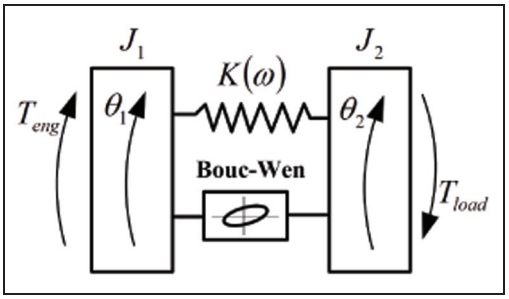

Figure 13. Nonlinear 2 degrees of freedom of the DMF.

moments of inertia of the primary and secondary flywheels, which are determined to be 1.191 and 0.092 kg m^2, respectively.

The Bouc–Wen model takes the following form

$$\dot{z}(t) = \alpha \cdot \dot{x}(t) - \beta|\dot{x}(t)||z(t)|^{n-1}z(t) - \gamma\dot{x}(t)|z(t)|^n \quad (24)$$

where α, β, γ, and n are the model parameters to be determined and $z(t)$ is the restoring frictional torque in this DMF. On the basis of the model described in Figure 13, $z(t)$ can be given by

$$z(t) = \frac{1}{2}\left(T_{eng}(t) + T_{load}(t) - J_1\ddot{\theta}_1(t) + J_2\ddot{\theta}_2(t)\right) - K(\omega)\cdot(\theta_1(t) - \theta_2(t)) \quad (25)$$

where $T_{load}(t)$ is the load torque, which is tested by the torque sensor on the side of the secondary flywheel; $x(t)$ is the torsional vibration angle between the primary and the secondary flywheels, that is, $x(t) = \theta_1(t) - \theta_2(t)$, which can be obtained from the dynamic experiment.

Levenberg–Marquardt method[15–17] is adopted to estimate the parameters. It has been proved that the Levenberg–Marquardt method is more robust and

Table 4. Estimated parameters.

Torque (N m)	Rotational speed (r/min)	α	β	γ	n	Error (%)
80	900	8.9512	0.7904	0.1023	2.4	7.73
	1500	12.9423	0.6073	0.0059	2.2	6.24
	2100	16.0552	0.3993	0.0053	2.4	10.21
120	900	8.9678	0.5904	0.0521	2.3	7.67
	1500	10.9862	0.6713	0.0512	2.4	9.36
	2100	14.9998	0.6924	0.0523	2.4	13.45

efficient than the widely used Gauss–Newton method.[18] The estimation scheme for the model parameters is divided to two steps:

Step 1. The exponential power n is given by a proper value at first. Moreover, the remaining parameters are estimated by the least square method.

The discrete torsional vibration and torque data can be obtained by the dynamic experiment, which are $\{T_{eng,i}\}$, $\{T_{load,i}\}$, $\{\theta_{1,i}\}$, and $\{\theta_{2,i}\}$ with the same sampling frequency, where $i = 1, 2, \ldots, j, \ldots, N$, and N denotes the length of the signal. Assume the time interval being Δt, $\theta_{1,i} = \theta_1(i \cdot \Delta t)$ and $\theta_{2,i} = \theta_2(i \cdot \Delta t)$. Hence, $x_i = \theta_{1,i} - \theta_{2,i}$. Solving the definite integral of equation (24) from t_1 to t_j, each term of the equation can be rewritten as

$$\int_{t_1}^{t_j} \dot{z}(t)dt = z(t)|_{t_1}^{t_j} = z_j - z_1 = b \tag{26}$$

$$\alpha \int_{t_1}^{t_j} \dot{x}(t)dt = \alpha x(t)|_{t_1}^{t_j} = \alpha\left(x_j - x_1\right) = \alpha I_1 \tag{27}$$

$$\beta \int_{t_1}^{t_j} |\dot{x}(t)||z(t)|^{n-1} z(t)dt = \beta \cdot \frac{1}{2}\left(\sum_{i=1}^{j}\left(|\dot{x}_{i+1}| \cdot z_{i+1} \cdot |z_{i+1}|^{n-1} + |\dot{x}_i| \cdot z_i \cdot |z_i|^{n-1}\right) \cdot \Delta t\right) = \beta \cdot I_2 \tag{28}$$

$$\gamma \int_{v}^{t_j} \dot{x}(t)|z(t)|^n dt = \gamma \cdot \frac{1}{2}\left(\sum_{i=1}^{j}\left(\dot{x}_{i+1} \cdot |z_{i+1}|^n + \dot{x}_i|z_i|^n\right) \cdot \Delta t\right) = \gamma \cdot I_3 \tag{29}$$

Thus, $b = \alpha I_1 + \beta I_2 + \gamma I_3$. Using the least square method, the parameters of α, β, and γ can be estimated.

Step 2. Taking the parameters determined in step 1 as the initial iterative vector, the Levenberg–Marquardt algorithm is implemented. The dynamic experimental data shown in Figure 4 will be used to estimate the model parameters $\{\alpha, \beta, \gamma, n\}$. The estimation errors can be determined by equation (30)

$$E_z = \left[\frac{\sum_{k=1}^{M} |z_k - \tilde{z}_k|^2}{\sum_{k=1}^{M} |z_k|^2}\right] \tag{30}$$

where M is the number of selected j in step 1. z_k and $\tilde{z}_k$ are experimental torque and estimated torque, respectively. Using the initial guess, $n = 1$, the estimated results by the above approach are given in Table 4, and the hysteretic curves using these parameters are plotted in Figure 14, which are also compared with the experimental results. The results show that the selected Bouc–Wen model can fit well the experimental data from Figure 4.

Conclusion

It is experimentally verified that the nonlinear hysteretic and rotational speed-dependent phenomenon exists in a long-arc spring DMF. Centrifugal force results in the rotational speed-dependent frictional force and then the nonlinear stiffness of this kind of the DMF. Considering the transferred torque as an overlying form of nonlinear elastic torque and the hysteretic frictional torque, a nonlinear 2-degree-of-freedom torsional vibration system for this DMF is presented in this work. The nonlinearity of stiffness and the hysteretic model of frictional torque are specifically investigated. A stiffness model of rotational speed is derived, according to the static mechanic model and the static experimental data. The Bouc–Wen model is adopted to model the hysteretic frictional torque. Incorporating the elastic torque and using the dynamic experimental data, the model parameters are estimated by

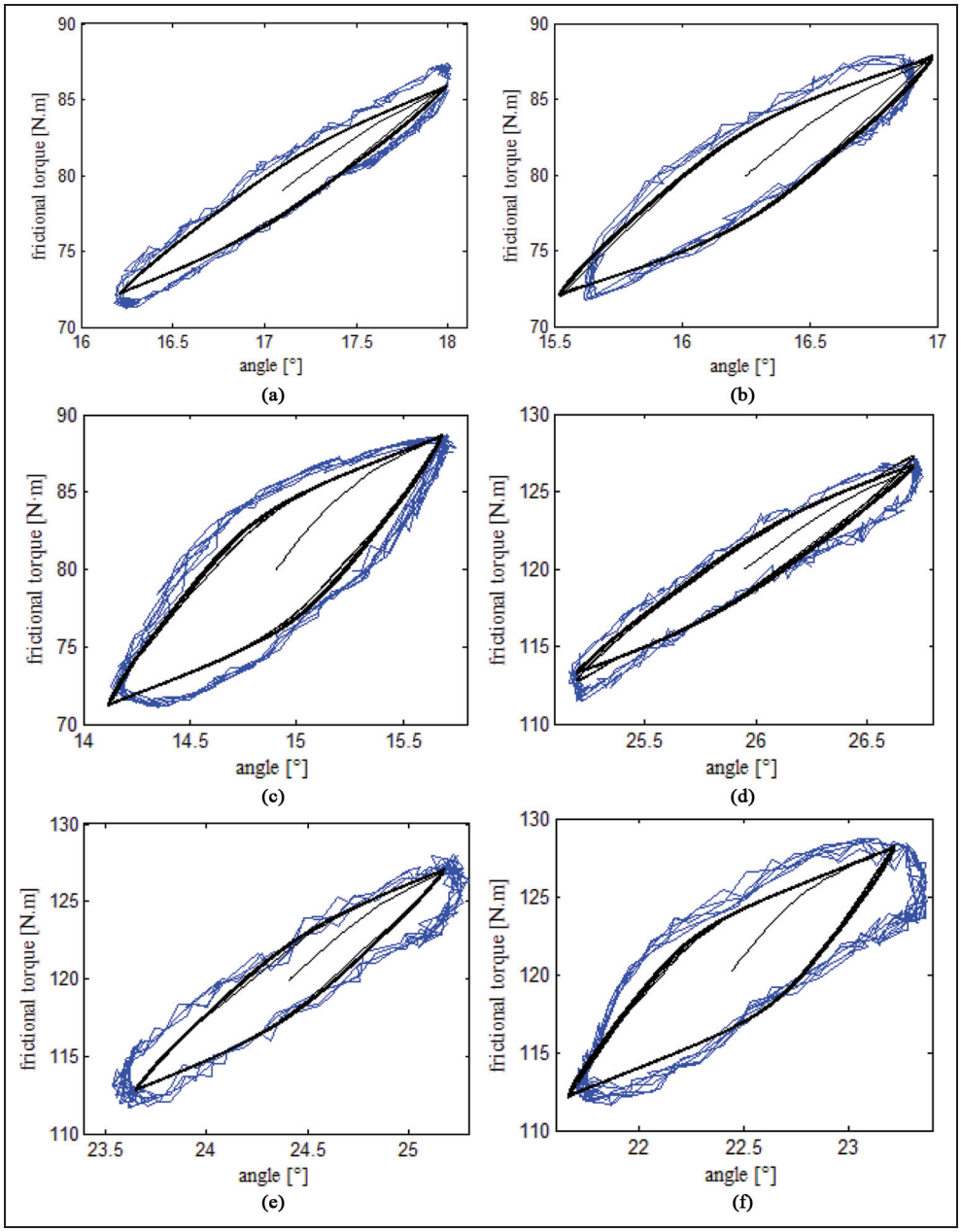

Figure 14. Hysteretic curves by Bouc–Wen model: (a) 80 N m, 900 r/min; (b) 80 N m, 1500 r/min; (c) 80 N m, 2100 r/min; (d) 120 N m, 900 r/min; (e) 120 N m, 1500 r/min; and (f) 120 N m, 2100 r/min.

Levenberg–Marquardt method. The estimated results show that the presented model can accurately describe the hysteretic characteristics.

Declaration of conflicting interests

The authors declare that there is no conflict of interest.

Funding

This work was supported by National Natural Science Foundation of China under Grant 51405355.

References

1. Isaac HY, Jia-Shiun C, Keith DM, et al. NVH analysis of balancer chain drives with the compliant sprocket of the crankshaft with a dual-mass-flywheel for an inline-4 engine. In: *Noise and vibration conference and exhibition*, St. Charles, IL, 15–17 May 2007, SAE Technical Paper 2007-01-2415.
2. Walter A, Kiencke U, Jones S, et al. Anti-Jerk & idle speed control with integrated sub-harmonic vibration compensation for vehicle with dual mass flywheel. *SAE Int J Fuel Lubr* 2009; 1: 1267–1276.

3. Walter A, Kiencke U, Jones S, et al. Misfire detection for vehicles with Dual Mass Flywheel (DMF). In: *14th Asia Pacific SAE automotive engineering conference*, Los Angeles, CA, 5–8 August 2007, SAE Technical Paper 2007-01-3544.
4. Walter A, Brummund S, Merz B, et al. Estimation of the instantaneous engine torque for vehicles with dual mass flywheel. In: *5th IFAC symposium on advances in automotive control*, vol. 5, 20 August 2007, pp.167–174, http://www.ifac-papersonline.net/Detailed/39029.html
5. Lei C, Ming-Ran D and Zhengfeng J. Optimization method of performance parameters of dual mass flywheel. *Trans CSICE* 2012; 30: 277–283.
6. Schnurr M. Development of super-long-travel dual mass flywheel. In: *4th international clutch symposium*, Baden-Baden, 1990, pp.55–80. Baden: LuK GmbH & Co.
7. Albers A. Advanced Development of Dual Mass Flywheel (DMFW) design. In: *5th Luk symposium*, Bühl, 1994, pp.1–38. Baden: LuK GmbH & Co.
8. Schaper U, Sawodny O, Mahl T, et al. Modeling and torque estimation of an automotive dual mass flywheel. In: *2009 American control conference*, vol. 16, issue 6, St. Louis, MO, 10–12 June 2009, pp.1207–1212. New York: IEEE.
9. Shizhu W. *Tribology*. 3rd ed. Beijing, China: Tsinghua University Press, 2008.
10. Marcia Marie M and Denil KT. Consideration of Stribeck diagram parameters in the investigation on wear and friction behavior in lubricated sliding. *J Braz Soc Mech Sci* 2007; 29: 56–62.
11. Yinghui Z, Huihang L and Decheng W. *Spring manual*. 2nd ed. Beijing, China: China Machine Press, 2008.
12. Yong Z. *Parameter identification of Bouc-Wen hysteresis model and its application in elevator vibration modeling*. Master's Thesis, Shanghai Jiao Tong University, Minhang, China, 2008.
13. Bouc R. Forced vibration of mechanical system with hysteresis. In: *Proceedings of the fourth conference on nonlinear oscillations*, Prague, 5–9 September 1967, p.315. Prague: Academic Publishing.
14. Wen YK. Method for random vibration of hysteretic system. *J Eng Mech Div* 1976; 76: 249–263.
15. Madsen K, Nielsen HB and Tingleff O. *Methods for nonlinear least squares problems*. Kongens Lyngby: Informatics and Mathematical Modeling, Technical University of Denmark, 2004.
16. Kelley CT. *Iterative methods of linear and nonlinear equations*. Philadelphia, PA: SIAM, 1995.
17. Hoon W, Yoon-Young K, Haeil J, et al. Nonlinear rate-dependent stick-slip phenomena: modeling and parameter estimation. *Int J Solid Struct* 2001; 38: 1415–1431.
18. Mottershead JE and Stanway R. Identification of nth-power velocity damping. *J Sound Vib* 1986; 105: 309–319.